2750 *Chem. Mater.* **2010,** *22,* 2750–2756
DOI:10.1021/cm903633w

CHEMISTRY OF MATERIALS
Article

Synthesis and Properties of Turbostratically Disordered, Ultrathin WSe_2 Films

Ngoc T. Nguyen,[†] Polly A. Berseth,[†] Qiyin Lin,[†] Catalin Chiritescu,[‡] David G. Cahill,[‡] Anastassios Mavrokefalos,[§] Li Shi,[§] Paul Zschack,[⊥] Michael D. Anderson,[†,#] Ian M. Anderson,[#] and David C. Johnson*[,†]

[†]*Chemistry Department and Materials Science Institute, University of Oregon, Eugene, Oregon 97403,* [‡]*Department of Materials Science and Engineering, Frederick Seitz Materials Research Laboratory, University of Illinois, Urbana, Illinois 61801,* [§]*Department of Mechanical Engineering, The University of Texas at Austin, Austin, Texas 78712,* [⊥]*Advanced Photon Source, Argonne National Laboratory, Argonne, Illinois 60439, and* [#]*Surface and Microanalysis Science Division, National Institute of Standards and Technology, Gaithersburg, Maryland 20899*

Received December 1, 2009. Revised Manuscript Received February 8, 2010

Turbostratically disordered tungsten diselenide (WSe_2) thin films with as few as two *c*-axis-oriented (basal plane) structural units were synthesized from modulated elemental reactants. By varying the number of elemental W−Se bilayers deposited, the thickness could be controllably varied from two to eighty such structural units. The sample roughness decreases with increasing annealing time and temperature as the crystalline WSe_2 basal plane units self-assemble from the amorphous precursors. Low-angle X-ray diffraction data show that the thickness of the WSe_2 films is highly uniform after annealing, with estimated roughness of less than 0.2 nm, and highly oriented, with the *c* axis of the structural units oriented within 0.1° of the substrate normal as determined from rocking curves of the specular *00L*-type diffraction peaks. Pole figures of *hk*0-type reflections indicate that *c*-axis-oriented basal plane structural units are randomly oriented within the a-b plane. The widths of diffraction peaks of type *hk*0, 00*L*, and *hkl* ($h, k \neq 0; l \neq 0$) indicate coherence lengths of about 6−7 nm in the *a*−*b* plane, the full thickness of the film along the *c* axis, and 1−2 nm in mixed-index directions. Scanning transmission electron microscopy imaging corroborated the X-ray scattering results, providing direct evidence of strong *c*-axis texture, rotational disorder between adjacent basal plane structural units, and an intraplanar grain size of several nanometers. The combination of intraplanar crystallinity and interplanar rotational disorder explains the significant anisotropy of the thermal conductivity, which is 20−30 times higher in the *a*−*b* plane than along the *c* axis. Electrical measurements within the *a*−*b* plane indicate that the films exhibit n-type semiconducting behavior.

Introduction

Transition metal dichalcogenides exhibit novel behaviors that originate in part from their quasi two-dimensional (2D) structure. Interesting physical properties of this family of compounds include superconductivity, charge density waves, and magnetism; interesting chemical phenomena include intercalation, exfoliation, and photochemistry.[1−5] Transition metal dichalcogenides, MX_2, have a planar structural unit, corresponding to the basal plane in a hexagonal space group, that is comprised of a hexagonal array of group IV, V, or VI transition metal cations (M) sandwiched between two hexagonal close-packed layers of chalcogen anions (X = S, Se, or Te). The coordination of the transition metal cations within these X−M−X basal plane structural units can be octahedral, corresponding to an AbC stacking, or trigonal prismatic, with an AbA stacking, depending on the relationship between the chalcogen layers. (Here we use the convention that the stacking of the anion and cation sublattices are distinguished by representing the former in capital letters.) These basal plane structural units stack in a wide variety of sequences to form different polymorphs within a large family of compounds with the common chemical formula MX_2. For example, the simplest 2H polymorph corresponds to an AB stacking of the structural units. Intralayer bonding is strong, with metal cations covalently bonded to six chalcogen anions, whereas interlayer bonding is weak, with adjacent basal plane structural units bonded to each other by van der Waals forces. The anisotropic nature of the bonding results in a growth morphology of 2D sheets with easy cleavage normal to the growth direction, which has enabled researchers to prepare single-unit-cell-thick layers by mechanical means.[6]

*Corresponding author. E-mail: davej@uoregon.edu.

(1) Wilson, J. A.; Yoffe, A. D. *Adv. Phys.* **1969**, *18*, 193.
(2) Friend, R. H.; Yoffe, A. D. *Adv. Phys.* **1987**, *36*, 1.
(3) Cabrera, C. R.; Abruna, H. D. *Proc.−Electrochem. Soc.* **1988**, *88*, 258.
(4) Wilson, J. A.; Di Salvo, F. J.; Mahajan, S. *Adv. Phys.* **1975**, *24*, 117.
(5) Schaak, R. E.; Mallouk, T. E. *Chem. Commun.* **2002**, *7*, 706.
(6) Novoselov, K. S.; Jiang, D.; Schedin, F.; Booth, T. J.; Khotkevich, V. V.; Morozov, S. V.; Geim, A. K. *Proc. Natl. Acad. Sci. U.S.A.* **2005**, *102*, 10451.

Published on Web 03/19/2010

Tungsten diselenide (WSe_2) is a well-known semiconductor within this family of compounds.[7,8] As prepared from high temperature reaction of element powders, the W exhibits trigonal planar coordination by the Se and the basal plane structural units stack in a 2H polymorph. Single crystals grown using vapor transport methods have been studied extensively as a potential candidate for photovoltaic application with reported cell efficiencies as high as 17% and excellent long-term stability.[9] Similarly grown single crystals of WSe_2 have also been used as a base component for high-mobility field effect transistors (FETs) in a "flexible" electronic device,[10] taking advantage of its high charge carrier mobility and mechanical flexibility. Recently, WSe_2 has been reported to exhibit extraordinarily low thermal conductivity when prepared in a manner that results in substantial rotational (turbostratic) disorder between adjacent Se−W−Se basal plane structural units.[11]

Many other synthesis methods have been used to prepare WSe_2 besides direct reaction of elemental powders,[12,13] including physical vapor deposition,[14] reduction from metal triselenide,[15] soft selenization of a W film,[16] chemical vapor deposition,[17−19] and pulsed electrodeposition from H_2WO_4 and SeO_2 under galvanostatic conditions.[20] These methods yield WSe_2 with selenium-to-tungsten atomic ratios of between 1.99 and 2.00, *c*-axis lattice parameters of between 1.295 and 1.323 nm, *a*-axis lattice parameters of between 0.318 and 0.339 nm, and a reported band gap of between 1.3 and 1.775 eV.[7] The variability of these parameters is consistent with the nonequilibrium nature of the products obtained from some of these synthetic approaches, as the phase diagram indicates that WSe_2 is a line compound with a very narrow range of compositional stability. Growth of single crystals of WSe_2 is typically performed via vapor phase transport, a slow batch process. All of these synthetic approaches typically yield the 2H polymorph of WSe_2.

Here we describe a self-assembly approach for the synthesis of ultrathin films of a turbostratically disordered polymorph of WSe_2 with thickness control at the level of individual basal plane structural units. The synthesis is accomplished through the deposition of alternating subnanometer-thick layers of elemental reactants with thicknesses precisely calibrated such that each deposited bilayer forms an individual basal plane structural unit of WSe_2 upon annealing. We describe this as self-assembly because the basal plane structural units of WSe_2 form turbostratically disordered layers held together by weak van der Waal forces. The temperatures used are well below that typically used to synthesize WSe_2 and the product is not the most thermodynamically stable form at the temperatures investigated. A schematic representation of the film evolution is shown in Figure 1. The extraordinarily small *c*-axis (interplanar) thermal conductivity of this polymorph of WSe_2 has been reported previously.[11] Here we detail the synthesis, structure, and composition as well as the intraplanar thermal and electrical properties of this new polymorph.

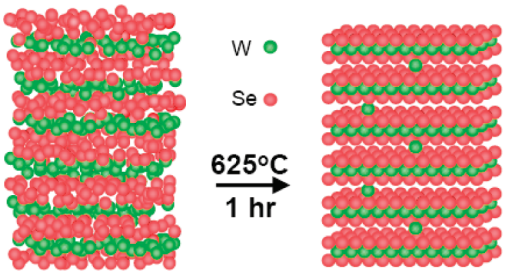

Figure 1. Schematic representation of modulated elemental reactant WSe_2 thin film, as deposited and following annealing.

Experimental Section

The samples were prepared in a custom-built high vacuum deposition system, as described elsewhere.[21] The tungsten was deposited with an electron beam gun at a rate of 0.02 nm/s and selenium was deposited with an effusion cell at a rate of 0.05 nm/s. A quartz crystal monitoring system placed 25 cm above each source was used to control deposition rates, and the length of time a shutter was left open controlled elemental layer thicknesses. The sample precursors were deposited onto (001)-oriented single-crystal silicon wafers at ambient temperature for X-ray diffraction (XRD) and X-ray reflectivity (XRR) studies, and onto polished fused silica slides for electrical measurements. The substrates were rinsed with acetone followed by ethanol prior to deposition. Samples were annealed under an inert nitrogen atmosphere to promote self-assembly of crystalline WSe_2 from the amorphous precursors. The silicon wafers had a variety of oxide thicknesses. Tungsten silicide formation was not observed when annealing below 700 °C.

Deposition parameters were calibrated to yield the appropriate stoichiometry and absolute number of atoms required for the formation of individual WSe_2 basal plane structural units from each deposited W−Se bilayer. The calibration was accomplished through a three-step process. The first step is designed to achieve coarse calibration of film composition. The deposition of one elemental reactant is systematically varied as that of the other elemental reactant is held constant. The calibration

(7) Deshpande, M. P.; Solanki, G. K.; Agarwal, M. K. *Mater. Lett.* **2000**, *43*, 66.
(8) Kam, K.; Parkinson, B. A. *J. Phys. Chem.* **1982**, *86*, 463.
(9) Prasad, G.; Srivastava, O. N. *J. Phys. D: Appl. Phys.* **1988**, *21*, 1028.
(10) Podzorov, V.; Gershenson, M. E. *Los Alamos National Laboratory, Preprint Archive, Condensed Matter* **2004**, *1−3*, 0401243.
(11) Chiritescu, C.; Cahill, D. G.; Nguyen, N.; Johnson, D.; Bodapati, A.; Keblinski, P.; Zschack, P. *Science* **2007**, *315*, 351.
(12) Merzhanov, A. G.; Borovinskaya, I. P.; Ratnikov, V. I.; Prokudina, V. K.; Memelov, V. L.; Gluskin, Y. A. *Izv. Akad. Nauk SSSR, Neorg. Mater.* **1977**, *13*, 811.
(13) Zelikman, A. N.; Kalikham, V. L.; Krein, O. E.; Lobova, T. A.; Gladchenko, E. P.; Duksina, A. G. *Izv. Akad. Nauk SSSR, Neorg. Mater.* **1970**, *6*, 1930.
(14) Kershaw, R.; Vlasse, M.; Wold, A. *Inorg. Chem.* **1967**, *6*, 1599.
(15) Nath, M.; Rao, C. N. R. *Chem. Commun.* **2001**, *21*, 2236.
(16) Salitra, G.; Hodes, G.; Klein, E.; Tenne, R. *Thin Solid Films* **1994**, *245*, 180.
(17) Deshpande, M. P.; Patel, P. D.; Vashi, M. N.; Agarwal, M. K. *J. Cryst. Growth* **1999**, *197*, 833.
(18) Traving, M.; Boehme, M.; Kipp, L.; Skibowski, M.; Starrost, F.; Krasovskii, E. E.; Perlov, A.; Schattke, W. *Phys. Rev. B: Condens. Matter* **1997**, *55*, 10392.
(19) Schimmel, T.; Kueppers, J.; Lux-Steiner, M. *Thin Solid Films* **1995**, *264*, 212.
(20) Delphine, S. M.; Jayachandran, M.; Sanjeeviraja, C. *Mater. Chem. Phys.* **2003**, *81*, 78–83.
(21) Fister, L.; Li, X.-M.; McConnell, J.; Novet, T.; Johnson, D. C. *J. Vac. Sci. Technol., A* **1993**, *11*, 3014.

constant (tooling factor), relating the frequency shift of the quartz crystal monitor to the deposited film thickness, is determined structurally by XRR and chemically by electron probe microanalysis (EPMA), as described below. The second step is designed to establish a coarse calibration of the absolute thickness of the deposited bilayer necessary to form a single basal plane structural unit of the WSe_2. A second set of films is deposited using the ratio of elemental reactants established in step one, but while systematically varying the thickness. XRR and EPMA were performed on the as-deposited films to probe possible effects of changes in the sticking coefficients of the elemental reactants with deposition time for these ultrathin layers and on subsequently annealed films to monitor volume changes during self-assembly of the basal plane structural units from the elemental reactants. The third and final step provides a fine calibration of the deposition parameters to achieve maximum crystallinity of the self-assembled WSe_2 films following annealing. A final series of films is prepared while systematically varying the deposition time of one of the elemental reactants in the vicinity of the absolute deposition parameters established in step two. The optimal deposition parameters are then chosen as those achieving the maximum intensity of the diffraction peak corresponding to 2H-WSe_2 002 reflection. An arbitrary number, n, of repetitions of these calibrated W−Se elemental reactant bilayers can then be performed to achieve a film with n basal plane structural units.

Chemical composition was determined using a Cameca S-50 electron probe microanalyzer and the Stratagem data analysis program[22] using a beam current of 20 nA and beam voltages of (8, 12, and 16 kV). X-ray wavelength dispersive spectrometry was performed using pure elements or compounds of known stoichiometry as standards. Ten independent measurements at different sample positions were averaged to determine the final composition. Less than 2 at % oxygen was detected.

The crystalline quality, orientation, and thickness of the films were evaluated by high-resolution XRD and XRR using a Bruker D8 Discover diffractometer with Cu $K_{\alpha 1}$ radiation and Göbel mirror, Bragg−Brentano optics geometry. Synchrotron X-ray powder diffraction patterns were also measured at the high-resolution 33ID beamline of the Advanced Photon Source (APS) at Argonne National Laboratory. The sample was mounted on a four-circle Huber goniometer. In the synchrotron experiments, two wavelengths of 121.7 and 124.1 pm were used (at and below the W L_3 absorption edge) for anomalous XRD scans to refine the z-axis coordinates of the anion and cation sublattices within the basal plane structural units. Intraplanar diffraction data were collected with a shorter wavelength of 67.02 pm. The diffraction data collected at different energies were refined using the General Structure Analysis System (GSAS).[23] Diffraction data were collected in the range $12° \leqslant 2\theta \leqslant 50°$ with a step increment of 0.005° and a 1 s acquisition time per step.

Cross sectional specimens for scanning (STEM) and conventional (TEM) transmission electron microscopy analysis were prepared using the small angle cleavage technique,[24] followed by final cleaning and thinning using an FEI NOVA Nanolab DualBeam FIB equipped with a Sidewinder ion column. Samples were thinned to approximately 300 nm using 30 kV accelerating voltage on the ion source followed by a polishing step at 5 kV and final end pointing at 2 kV. Samples were plasma cleaned using a Fischione Instruments model 1020 plasma cleaner for 5 min prior to analysis to remove any organic contamination.

Analytical electron microscopy measurements were performed using an FEI Titan STEM/TEM equipped with a double-hexapole spherical aberration (C_s) corrector on the probe forming lens and operating at 300 kV. Images were collected using a condenser beam convergence semiangle of $\alpha = 18$ mrad and a high angle annular dark-field (HAADF) detector with an inner semiangle of $\beta = 60$ mrad. Imaging was conducted by first orienting the specimen to the [110] zone axis of the silicon substrate, followed by a lateral stage shift to the site of interest. Orientation at the [110] zone axis of silicon places the cross section of the film normal to the optic axis of the microscope. Image analysis was conducted using the ImageJ for Microscopy suite of plug-ins. Distances were measured using the line tool and the plot profile feature on the calibrated image. A large line width was chosen to provide an average distance over many atomic columns. Special care was taken to ensure that the line was perpendicular to the film cross-section during the measurement.

The thermal conductivities of the thin films in directions perpendicular (interplanar) and parallel (intraplanar) to the substrate were measured using different techniques. Interplanar thermal conductivity was measured using time-domain thermoreflectance, as reported previously.[11] Intraplanar thermal conductivity was directly measured on a suspended film using a microfabricated measurement device with integrated heaters and thermometers.[25,26] Briefly, a rectangular section of film was defined using photolithography and a fluoride-based dry etch procedure. This rectangular section of film was then lifted off of the substrate using a nanomanipulator and placed between two membrane thermal reservoirs of the measurement device. Focused electron beam induced deposition of platinum was used to clamp the strip onto the two membranes. Electrical heating was used to increase the temperature of one membrane of the device and a temperature increase in the other membrane can be measured because of heat conduction through the film sample. Finally, resistivity measurements were performed using a four-point probe van der Pauw configuration.

Results and Discussion

The calibration of the elemental reactant deposition parameters was unambiguous. A plot of the XRD intensity of 2H-WSe_2 002 peak as a function of the deposition time of the W elemental reactant at constant Se deposition time, used to perform the third and final step of the calibration, is shown in Figure 2. The plot reveals a strongly peaked intensity curve as a function of tungsten deposition time. The optimal composition after annealing is slightly (~6%) Se rich relative to an ideal WSe_2 stoichiometry.

Film thicknesses, WSe_2 basal plane structural unit pitches, and compositions of thin film samples, both as-deposited and following annealing at 625 °C, are

(22) Certain commercial equipment, instruments, or materials are identified in the document. Such identification does not imply recommendation or endorsement by the National Institute of Standards and Technology, nor does it imply that the products are necessarily the best available for the purpose.
(23) Larson, A. C.; Von Dreele, R. B. *General Structure Analysis System*; Los Alamos National Laboratory: Los Alamos, NM, 2004.
(24) Walck, S. D.; McCaffrey, J. P. *Thin Solid Films* **1997**, *308−309*, 399.
(25) Shi, L.; Li, D.; Yu, C.; Jang, W.; Kim, D.; Yao, Z.; Kim, P.; Majumdar, A. *J. Heat Transfer* **2003**, *125*, 881.
(26) Mavrokefalos, A.; Nguyen, N. T.; Pettes, M. T.; Johnson, D. C.; Shi, L. *Appl. Phys. Lett.* **2007**, *91*, 171912.

summarized in Table 1 for selected samples with a variety of optimized bilayer deposition cycles, n. X-ray reflectivity patterns collected from several of the as-deposited thin film samples are shown in Figure 3. The patterns of samples with numerous deposited bilayers contain a peak at $2\theta \approx 11.5°$ that corresponds to the compositional modulation of elemental W and Se in the as-deposited films, as well as a broad diffraction peak centered at $2\theta \approx 13°$, where the 002 Bragg diffraction peak for 2H-WSe_2 would be expected. The patterns also contain Kiessig fringes, which are subsidiary maxima resulting from X-ray interference from the front and back of the films. In the as-deposited films, the Kiessig fringes are observed out to $2\theta \approx 10°$ in thin films with relatively few deposited bilayers, n, and out to approximately $2\theta \approx 8°$ in thicker films with larger n. Parratt has derived a relationship between film smoothness and the maximum angle at which these fringes are observed:[27]

$$\Delta t = \frac{\lambda}{4(\theta_i^2 - \theta_c^2)^{1/2}}$$

where Δt is the film roughness, λ is the X-ray wavelength (in our case Cu Kα), θ_i is the maximum angle at which Kiessig fringes are resolved, and θ_c is the critical angle. For films where fringes are observed out to $2\theta \approx 10°$, the calculated film thickness variations are $\Delta t = 0.4$ nm, whereas for the thicker films, the calculated film thickness variations are $\Delta t = 0.7$ nm. In the high-angle diffraction patterns for thicker as-deposited films, we observed broad maxima (~2−4° full width at half-maximum intensity) at angles corresponding to the 002, 004, 006, and 008 Bragg reflections of 2H-WSe_2. These broad maxima indicate that the self-assembly of basal plane structural units from the amorphous elemental precursors has already begun to occur during deposition.

Diffraction data collected as a function of annealing temperature for the thickest deposited film, $n = 80$, are shown in Figure 4. The data indicate that significant structural changes occur during the annealing process. A gradual shift in the low-angle Bragg diffraction maxima to higher angles indicates that the film thickness decreases by approximately 20% upon annealing as the films crystallize and as excess Se is lost due to sublimation. As a result of the contraction of the film during self-assembly of the basal plane structural units, the diffraction maxima from the layering become coincident with the diffraction maxima expected for the 002, 004, 006, and 008 reflections of tungsten diselenide after annealing at 625 °C. X-ray reflectivity and diffraction patterns of annealed films with a variety of thicknesses are shown in

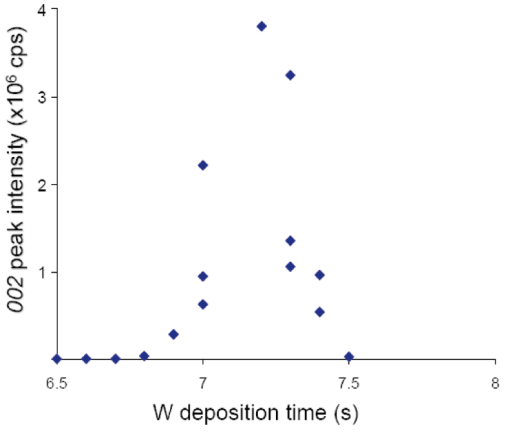

Figure 2. 2H-WSe_2 002 peak intensity from annealed films as a function of W deposition time at constant Se deposition time. The intensity maximum was deemed the optimal W deposition time and used for the growth of subsequent films.

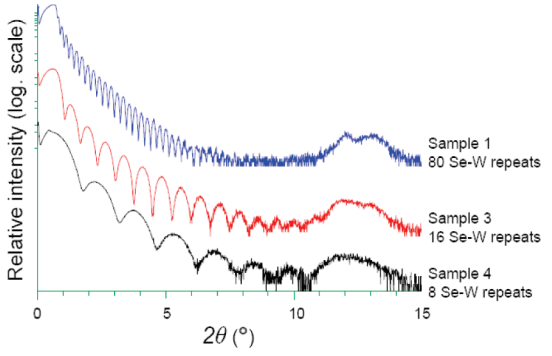

Figure 3. Low-angle X-ray diffraction patterns collected from as-deposited thin films containing $n = 80$, 16, and 8 W−Se reactant bilayers. The oscillations in intensity that occur in the angular range $1° \leq 2\theta \leq 10°$ result from X-ray interference from the top and bottom surfaces of the deposited films. The period of these oscillations can be used to determine the characteristic bilayer repeat distance, which is 0.85 nm for $n = 80$. The broad diffraction maxima at $2\theta \approx 12-13°$, which is the expected angle for the 002 reflection of WSe_2, suggest the presence of ordered basal plane structural units of WSe_2 in the as-deposited films.

Table 1. Thickness, Distance between Basal Planes of WSe_2 Structural Units, and Composition of Thin Film Samples with Selected Number of W−Se Bilayer Depositions, n, Both As-Deposited and Following Annealing at 625 °C[a]

					composition as-deposited (at %)		composition after annealing (at %)	
sample ID	n	thickness as-deposited (nm)	thickness after annealing (nm)	distance between WSe_2 basal planes (nm)	W	Se	W	Se
1	80	57.0(7)	53.2(2)	0.662(1)	26.3(5)	73.7(7)	31.9(4)	68.1(4)
2	50	38.0(7)	32.1(2)	0.662(1)	28.0(4)	72.0(6)	31.3(5)	68.7(7)
3	16	12.5(5)	10.6(2)	0.662(1)	26.0(3)	74.0(7)	31.2(7)	68.6(9)
4	8	6.7(5)	5.3(2)	0.665(5)	25.2(9)	74.8(9)	30.9(9)	69.1(9)
5	5	4.0(3)	3.3(2)	0.665(5)				
6	4	3.1(2)	2.6(2)	0.66(1)				
7	2	1.8(2)	1.4(2)					

[a] The uncertainties in the least significant digits are indicated in parentheses. Samples 5, 6, and 7 were too thin for accurate EPMA compositional measurement.

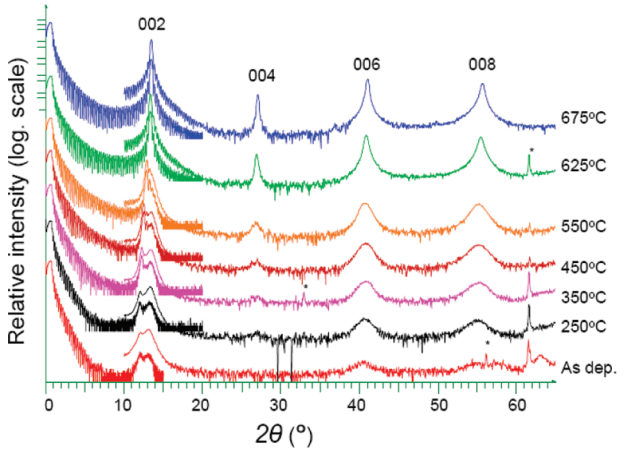

Figure 4. Diffraction data collected as a function of annealing temperature for Sample ID 1, $n = 80$. The film was annealed at each of the indicated temperatures for 1 h in a N_2 atmosphere with less than 1 μL L^{-1} O_2. The peak at $2\theta = 12°$ is characteristic of the repeat unit of the as-deposited elemental reactant bilayers. The broad peak at $2\theta = 13°$, at the angle expected for the 002 reflection of 2H-WSe_2, results from the presence of ordered basal plane structural units of WSe_2. Diffraction peaks marked with an asterisk (*) arise from the Si substrate.

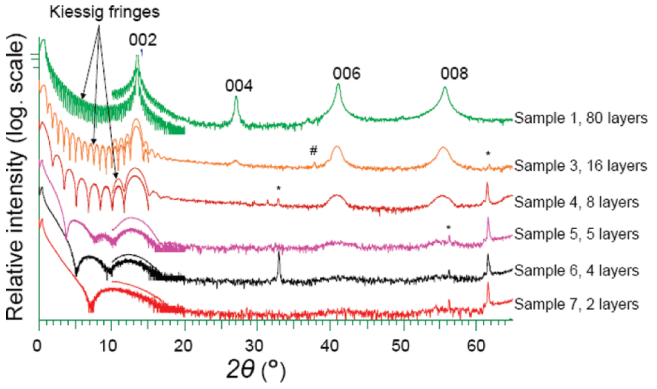

Figure 5. Low- and high-angle X-ray diffraction patterns of several WSe_2 thin films acquired with a conventional laboratory diffractometer. The data were collected after annealing the samples at 625 °C for 1 h in N_2. Diffraction peaks mark with an asterisk (*) and a pound sign (#) arise from the Si substrate and sample holder, respectively.

Figure 5. The reflectivity patterns show well-resolved Kiessig fringes over a larger range of angles than observed in the as-deposited films, to $2\theta \approx 17°$. The increase in θ_i indicates that the front and back surfaces and the internal dichalcogenide planes of the films become significantly more parallel, corresponding to a calculated thickness variation of $\Delta t = 0.2$ nm using the formula of Parratt. The high-angle diffraction maxima also become sharper upon annealing as the coherence between the dichalcogenide planes increases. The presence of diffraction peaks only at angles corresponding to the 00L family of Bragg peaks indicates that the basal planes of the WSe_2 structural units are aligned parallel to the substrate. This film orientation was confirmed by rocking curve scans that indicate that the basal planes are aligned to within 0.1° of the substrate. Calculating the coherence length perpendicular to the substrate using the Scherrer equation[28,29] yields values of 5, 10, and 53 nm for samples with $n = 8$, 16, and 80 respectively, suggesting that the basal planes of the dichalcogenide are coherently spaced throughout the thickness of the films. The calculated values of the mean thickness of the basal plane structural units range from 0.665 nm for the thinnest samples to 0.662 nm for the thicker samples. These calculated values are slightly larger than the reported c-axis lattice parameter of (0.65−0.66) nm for WSe_2.[20] In addition to the larger c-axis lattice parameter, the intensity of the 004 diffraction peak is also significantly enhanced compared to the relative intensities reported for the 002, 004, 006, and 008 reflections of 2H-WSe_2.

Rietveld refinement was performed using GSAS to model the structure along the c-axis using high-angle XRD data collected at and below the W L_3 absorption edge (10.189 and 9.989 keV, respectively) at the APS. The lowest symmetry hexagonal space group, $P\bar{3}m1$ (No. 164), was chosen for the refinement of the z-axis coordinate of the cation (W) and anion (Se) planes in the structure, because for $P\bar{3}m1$ the z-axis coordinate is independent of in-plane film texture. The refinement was performed iteratively, and the cycle was terminated when the residuals of both fitted peaks (R_f) and background (R_b) were less than 10% and χ^2 measure of goodness of fit was about 5. The results are shown in Figure 6. The refinement indicates that the cation (W) sublattice contains ~7% vacant sites in the sample examined, which is consistent the observed enhanced relative intensity of the 004 Bragg reflection. Modeled intercalation of up to 6 at % of W within the van der Waals gap did not improve the quality of the fit. These XRD results are in good agreement with elemental analyses performed by EPMA and Rutherford backscattering spectroscopy (RBS), which indicate that these samples are about 5% enriched in Se relative to the ideal 2:1 stoichiometry.

To examine the structure in crystallographic directions other than the c axis, diffraction data were collected throughout reciprocal space. Intraplanar[30] diffraction data collected at the APS on representative samples show that the films are well-crystallized within the a-b plane. Scans transverse through $hk0$-type reflections indicate long-range order within the a-b plane with grain sizes on the order of (6 to 7) nm. Analysis of the $hk0$ diffraction pattern collected from a film with $n = 50$ bilayers yielded an a-axis lattice parameter of (0.3290 ± 0.0002) nm, which is consistent with that reported for WSe_2. Diffraction scans along mixed index directions hkl ($h, k \neq 0; l \neq 0$) are very broad, yielding coherence lengths of ~2 nm or less, corresponding to no more than 3 basal plane structural units. Pole figure scans indicate that the films are polycrystalline, with the $a-b$ planes randomly oriented.

(27) Wainfan, N.; Parratt, L. G. *J. Appl. Phys.* **1960**, *31*, 1331.
(28) Scherrer, P., *Gottinger Nachrichten*, 1918.
(29) Klug, H. P.; Alexander, L. E. *X-Ray Diffraction Procedures for Polycrystalline and Amorphous Materials*, 2nd ed.; Wiley-Interscience Publication: New York, 1974.
(30) Tanner, B. K.; Hase, T. P. A.; Lafford, T. A.; Goorsky, M. S. *Adv. X-ray Anal.* **2004**, *47*, 309.

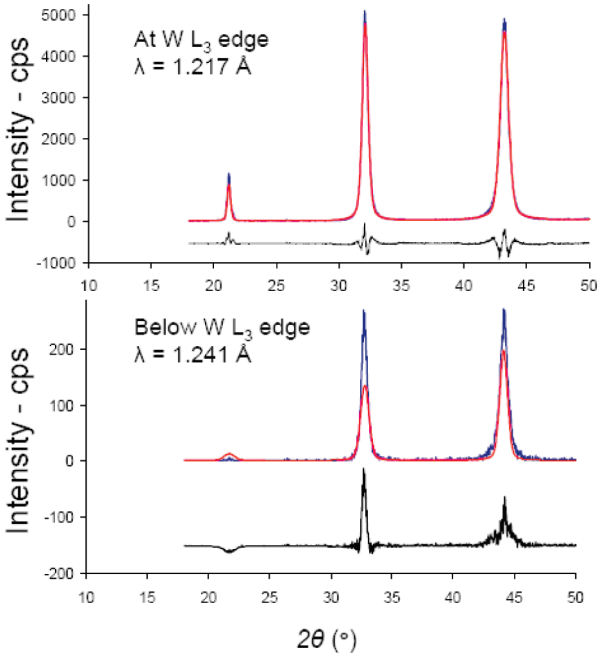

Figure 6. Results of XRD Rietveld refinements using X-ray energies near the W L_3 absorption edge. Parameter optimization is performed iteratively until residuals are less than 10% for fitted peaks (R_p) and background (R_b). The χ^2 measure of goodness of fit is around 5 for both refinements. The high χ^2 values arise from the finite film thickness, which is not taken into account during fitting. (Note: blue, collected data; red, fitted data; black, residuals.).

A representative STEM-HAADF image of the annealed WSe_2 films is shown in Figure 7. The image is of limited quality because of the beam sensitivity of the specimen; nevertheless, the image corroborates the structural information yielded by X-ray diffraction. Individual basal plane structural units are clearly resolved in the image. The parallel orientation of the planes, which coincide with the trace of the substrate in cross-section, is consistent with the strong *c*-axis texturing of the XRD patterns. The regularity in the spacing of these planes is consistent with the remarkable smoothness of the annealed films, consistent with the extended angular range over which Kiessig fringes are evident in the low-angle XRR scans. The sporadic appearance of atomic columns in domains localized to within a single basal plane structural unit and with a lateral extent of only a few nanometers, provides evidence of turbostratic disorder. The atomic columns of the hexagonal tungsten array, which dominate the contrast of the HAADF image, cannot be resolved at arbitrary grain orientations; however, the extent of regions exhibiting atomic columns, which indicate a grain orientation near a low-index zone axis, provide an indication of the grain size. Where they appear, these domains are localized to a single basal plane structural unit, consistent with the nanometer-scale coherence length measured by XRD peaks of mixed-plane indices, and with a lateral extent of only a few nanometers, consistent the intraplanar coherence length extracted from the rocking curves of *hk*0-type reflections.

Thermal conductivity measurements reveal that the unusual structure of the films is accompanied by equally

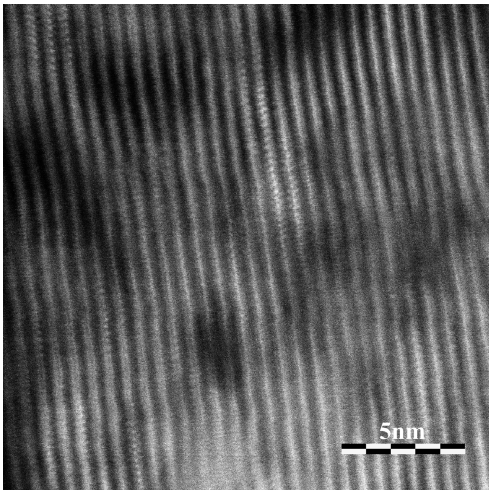

Figure 7. STEM-HAADF image of WSe_2 film in cross section. The image corroborates the structural information measured via XRD and XRR, including strong *c*-axis texturing, turbostratic disorder, and an intraplanar grain size of only a few nanometers.

unusual physical properties. Room-temperature interplanar thermal conductivities are found to range from (0.048 to 0.066) W m^{-1} K^{-1} for films of different thickness. These values are a factor of 30 smaller than that for single crystal WSe_2 measured by the same technique. The temperature dependence of the thermal conductivity is similar to that expected for an amorphous material.[11] This extraordinarily low thermal conductivity along the *c*-axis is thought to be a consequence of both the intraplanar crystallinity and the interplanar rotational disorder of the basal plane structural units. This hypothesis is supported by the increase in thermal conductivity as the intraplanar order is destroyed by ion irradiation[11] and the extensive structural characterization presented in this study. The intraplanar thermal conductivity value of the 160 nm thick film was measured to be about 1.6 $Wm^{1-}K^{-1}$, which is about 6 times smaller than the reported thermal conductivity of sintered pellets of WSe_2 within the *a*−*b* plane.[31] The higher intraplanar thermal conductivity is a consequence of the strong covalent bonding within the basal plane structural units. The anisotropy reported here for the thermal conductivity of turbostratically disordered WSe_2, a factor of ∼30, is significantly larger than the factor of 4.5 previously reported for WSe_2 powder.[32] To the best of our knowledge, only graphite with an anisotropy of 300 has a larger anisotropy in its thermal conductivity.[33]

Resistivity measurements using a four-point probe van der Pauw configuration show an activated temperature dependence consistent with semiconducting WSe_2 and electrical conductivities of ∼0.05 $(\Omega\,cm)^{-1}$ within the *a*−*b* plane at room temperature. Literature reports for the intraplanar electrical conductivity of WSe_2 vary over several orders of magnitude − from (1.2×10^{-4} to 4.0)

(31) Brixner, L. H. *J. Inorg. Nucl. Chem.* **1962**, *24*, 257.
(32) Troadec, J. P.; Bideau, D.; Guyon, E. *J. Phys. C: Solid State Phys.* **1981**, *32*, 4807.
(33) Lide, D. R., *CRC Handbook of Chemistry and Physics*, 83rd ed.; CRC Press: Boca Raton, FL, 2002−2003.

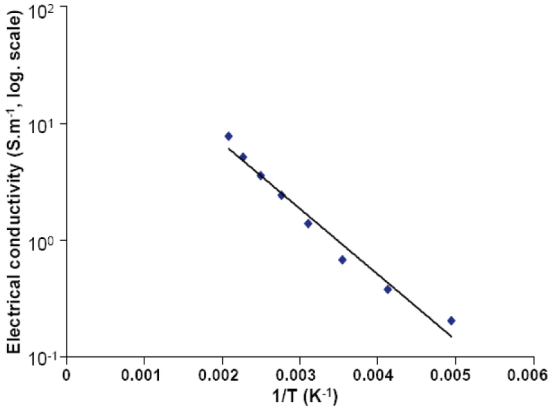

Figure 8. Temperature dependence of the electrical conductivity of a WSe_2 film. Semiconducting behavior is observed with an activation energy for conduction of 0.1 eV. The straight line is used to extract activation energy.

$(\Omega\,\mathrm{cm})^{-1}$ – because of differences in the concentration of impurities and defects introduced during different synthesis techniques.[31] The temperature dependence of the electrical conductivity of free-standing ribbons of WSe_2 is shown in Figure 8. An activation energy of 0.1 eV was calculated from the temperature dependence of the conductivity. This low activation energy, which is significantly less than the reported band gap of WSe_2, suggests that defect states provide the origin of the observed temperature dependence. The significant concentration of W vacancies suggested by the structural measurements with resonant XRD and the chemical measurements of EPMA and RBS may be the source of these defect states. Seebeck measurements reveal that our annealed films exhibit n-type semiconducting behavior, with Seebeck coefficients of around $-210\ \mu\mathrm{V\ K^{-1}}$. WSe_2 has been reported as exhibiting p-type behavior as prepared by most synthetic techniques involving stoichiometric reactions of the elements. N-type conductivity for WSe_2 was found in crystals grown with indium or copper as part of the reactant charge, in which case the behavior was ascribed to the incorporation of either Cu or In as intercalated atoms within the van der Waals gap and when Re is added as a substitutional dopant for W.[34,17] Single crystals grown with halogens as a transport agent are reported to be n-type presumably due to small amounts of halogen substituting for selenium. N-type conductivity has also been observed when Se is used as the transport agent,[35,36] in which case, similar to our samples, the n-type behavior likely arises from tungsten vacancies in the films.

(34) Kalikhman, V. L.; Umanskii, Y. S. *Soviet Phys. Usp.* **1973**, *15*, 728.
(35) Klein, A.; Dolatzoglou, P.; Lux-Steiner, M.; Bucher, E. *Sol. Energy Mater. Sol. Cells* **1997**, *46*, 175.
(36) Prasad, G.; Rao, N. N.; Srivastava, O. N. *Cryst. Res. Technol.* **1986**, *21*, 1303.

Conclusion

A series of turbostractically disordered WSe_2 films was prepared with precise integer control of the number of WSe_2 basal plane structural units. The synthesized films were extremely smooth and highly textured with the *c* axis oriented normal to the substrate. X-ray diffraction from the *a*–*b* planes and along the *c*-axis showed long-range crystalline order, whereas a coherence length of only (1 to 2) nm was observed in mixed-index *hkl* directions due to rotational disorder between basal plane structural units. This unusual structure results in an order of magnitude increase in the anisotropy of the thermal conductivity relative to that reported for WSe_2 powder. Electrical measurements show that the films exhibit n-type semiconducting behavior.

Acknowledgment. The research was funded by National Science Foundation under grant DMR 0103409 and supported by ONR Grants N00014-96-0407, N00014-05-1-0250, and N00014-1-1168. Thermal conductivity measurements were performed at the Laser and Spectroscopy Facility and the Center for Microanalysis of Materials of the Frederick Seitz Materials Research Laboratory, University of Illinois, which is partially supported by the U.S. Department of Energy under grant DEFG02-91-ER45439, and at the University of Texas at Austin Microelectronic Research Center, which is a node of the National Nanofabrication Infrastructure Network funded by NSF. The authors would like to thank Ms. Jenia Karapetrova at the Advanced Photon Source for assistance working on the beamline. Research at the Advanced Photon Source was supported by the U.S. Department of Energy, Office of Science, Office of Basic Energy Sciences, under the contract W-31-109-ENG-38.